Research Article | Vol. 31, No. 18 / 28 Aug 2023 / Optics Express 29074

Optics EXPRESS

Removing biases in dual frequency comb spectroscopy due to digitizer nonlinearity

NATHAN A. MALARICH,[1,5] KEVIN C. COSSEL,[1] JEAN-DANIEL DESCHENES,[2] FABRIZIO R. GIORGETTA,[1,3] BRIAN R. WASHBURN,[1] NATHAN R. NEWBURY,[1] JEROME GENEST,[4] AND IAN CODDINGTON[1,6]

[1] *National Institute of Standards and Technology, Spectrum Technology and Research Division, Boulder, CO 80305, USA*
[2] *Octosig Consulting, Quebec City, Quebec, Canada*
[3] *Department of Physics, University of Colorado Boulder, Boulder, CO 80309, USA*
[4] *Centre d'optique, photonique et laser, Universite Laval, Quebec, Quebec G1V 0A6, Canada*
[5] *nathan.malarich@nist.gov*
[6] *ian.coddington@nist.gov*

Abstract: Operation of any dual-comb spectrometer requires digitization of the interference signal before further processing. Nonlinearities in the analog-to-digital conversion can alter the apparent gas concentration by multiple percent, limiting both precision and accuracy of this technique. This work describes both the measurement of digitizer nonlinearity and the development of a model that quantitatively describes observed concentration bias over a range of conditions. We present hardware methods to suppress digitizer-induced bias of concentration retrievals below 0.1%.

1. Introduction

Dual-comb spectroscopy (DCS) generates a broadband spectrum that is in principle free of instrument lineshapes because each delta-function-like comb tooth has negligible power in adjacent spectral bins [1]. To first order this allows DCS to record undistorted broadband absorption spectra from which one can retrieve high-accuracy and high-precision concentration measurements. However, DCS is a Fourier transform technique based on recording a time-domain interferogram that can have an enormous amount of signal concentrated in a very small time, commonly dubbed the centerburst, followed by a very weak free induction decay extending to times well beyond the centerburst [2]. This creates a dynamic range problem as the entire interferogram must be recorded with a high level of linearity to avoid higher-order effects on the instrument lineshape and to achieve a low distortion spectrum [3–5].

Earlier work has shown that nonlinear behavior in the photodiodes used to detect the DCS interferograms can be a potential source of distortion, but this behavior can also be managed by chirping the lasers to spread out the centerburst and by photodetector design [6]. Here we show that the analog to digital converter (ADC) used to digitize the photodiode signal presents a similar obstacle to linearity and must be managed with equal care to avoid biases in the concentrations retrieved from DCS. This bias mitigation is particularly important for open-path sensing of greenhouse gases, which targets accuracies at the ~0.1% level [7].

ADCs commonly used in DCS can have different implementations but usually share some common properties. Generally, these devices have between 12 and 16 bit resolution and typically operate between 100 megasamples per second (MS/s) and 1000 MS/s [8–14]. As such they are usually pipeline ADCs composed of a small number of sequential flash ADC elements [15]. A high-level schematic of one of these devices is depicted in Fig. 1. Each flash element samples the signal with 3-4 bits of resolution and subtracts off the digitized value from the signal before passing the residual signal to the next flash element for finer measurement. The

#497497 https://doi.org/10.1364/OE.497497
Received 3 Jul 2023; accepted 31 Jul 2023; published 15 Aug 2023

Optics EXPRESS

nonlinear behavior of these devices is distinct from photo diodes and RF amplifiers in that ADCs are typically tuned to ensure a high level of linearity over the full device range, but the handoff between stages can introduce nonlinear behavior over smaller voltage scales, typically described as the integrated nonlinearity (INL).

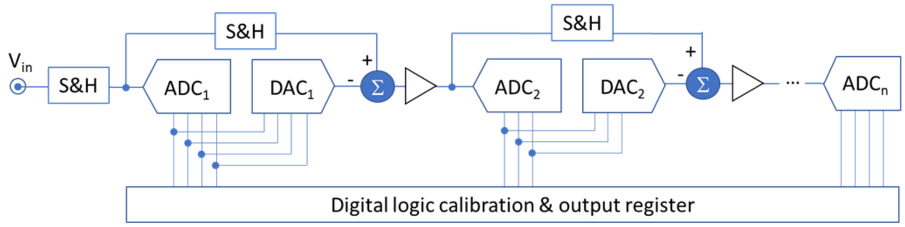

Fig. 1. Generalized schematic of a pipeline ADC. Successive flash ADCs with a few bits of resolution are cascaded. After each ADC a digital to analog converter (DAC) regenerates the voltage associated with the recorded bit value and subtracts it from the incoming signal. The residual is then amplified and passed to the next stage for digitization at finer resolution. S&H: sample and hold circuit.

In this work we accurately measure and model the impact of this integrated nonlinearity [16] on the subsequent concentration retrievals from DCS spectra, where it can cause biases exceeding 4%. We evaluate previous ways to deal with digitizer nonlinearity [17,18] and propose more effective solutions to wash out the effect of the INL. In all cases operating regimes are identified where the ADC induced concentration bias can support concentration retrievals at the 0.1% level even for an absorption signal where much of the free induction decay signal is less than one bit in amplitude.

2. Quantifying ADC integral nonlinearity

There are multiple approaches to measuring the INL of an ADC [19,20]. Here, we use an input sinewave, whose purity is ensured by the use of RF filters. Additionally, characterizing the exact amplitude of the sinewave is unnecessary here since overall ADC gain does not impact DCS signal quality. The ADCs tested here are the 14-bit, 250 MS/s Texas Instruments ADS62P49 [21], a common digitizer for DCS [17,22–24,28]. This ADC model has a specified INL of 2.5 bits and a specified effective number of bits (ENOB) of 11.3. Its input is AC-coupled with a voltage range from −1.285 V to +1.285 V, giving a least significant bit (LSB) value of 0.157 mV. The noise floor of this ADC has a measured 1.1 LSBs standard deviation.

To resolve the ADC transfer function (H_{ADC}) and the INL, 3×10^8 samples of a 9,999,500 Hz sine wave are recorded at 200 MS/s (Fig. 2) [20]. Because the sampling period and test waveform period have a very high least-common multiple, each of the 16386 ADC levels is sampled multiple times.

Optics EXPRESS

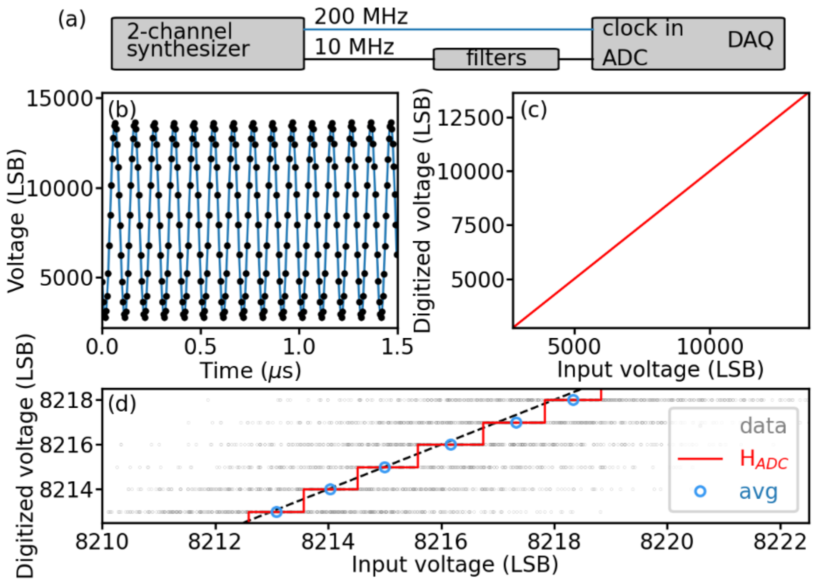

Fig. 2. Characterizing the ADC response with a sine wave. (a) Experiment schematic. A heavily filtered 9.9995 MHz sinewave test waveform and a 200 MHz clock frequency are generated on a 2-channel synthesizer. (b) The digitized sinewave (black dots) is fit to a sine function (blue trace) and fit values at each point are taken as the corresponding input voltage. (c) Plot of input vs recorded voltage showing the high degree of linearity over the full range. Both raw data (black dots) and our ADC transfer function (H_{ADC}), derived from the average of all input voltages associated with each ADC level and plotted in red) are shown though they are indistinguishable over this range. (d) Expanded view of (c). Here the ~2 LSB noise standard deviation of input voltages associated with each ADC level is visible. The average of this scatter at each level (blue circles) is used to calculate each step in H_{ADC}, seen in red. Small deviations of these average values from the black dashed parity line can been seen at this scale and represent the INL associated with this device.

The digitized sinewave is then fit to a sine function (Fig. 2(b)) and the fit values are taken to be the true input voltage for each sample. The mean of all input voltages recorded at each ADC level (Fig. 2(d) open circles) is then taken to be the center voltage of the transfer function H_{ADC} at that level. If the ADC response was perfectly linear, the plot of these two voltages (as seen in Fig. 2(d)) would lie on the (dashed) parity line. To better visualize the nonlinearity, the deviation from this parity line is plotted versus input voltage (Fig. 3), yielding the digitizer INL.

The nonlinearity of the ADC is most easily visualized as the INL, shown in Fig. 3. The nested sawtooth INL structure seen here is the result of the pipeline architecture of the ADC and seems to be common in these devices [19]. This 14-bit ADC determines the value of each bit in four serial stages of flash digitizers which appear to be 4 bits, 3 bits, 3 bits and 4 bits in resolution (Fig. 1). This successive handling of the voltage causes the nonlinearities in each stage to repeat across the full voltage range. Hence the sawtooth structures have a period of 10 bits (Fig. 3(a)) and 7 bits (Fig. 3(b)) and 4 bits (Fig. 3(c)). The slope of the sawtooth deviates more strongly from 1:1 over smaller voltage scales.

Due to this sawtooth structure in these ADCs, any signal spanning less than $\sim 2^7 = 128$ LSB can show a gain error of ~0.5%, while any signal smaller than ~4 bits or 16 LSB can have a gain error of ~3% compared to the full-scale gain. This gain error depends upon the location of the zero-voltage ADC level relative to the sawtooth structure. This zero-voltage level was observed to drift by as much as 8 LSBs over several hours (Fig. 3(c) markers). This drift was well within the ADC's specified zero-input voltage offset error of ±20 mV.

Optics EXPRESS

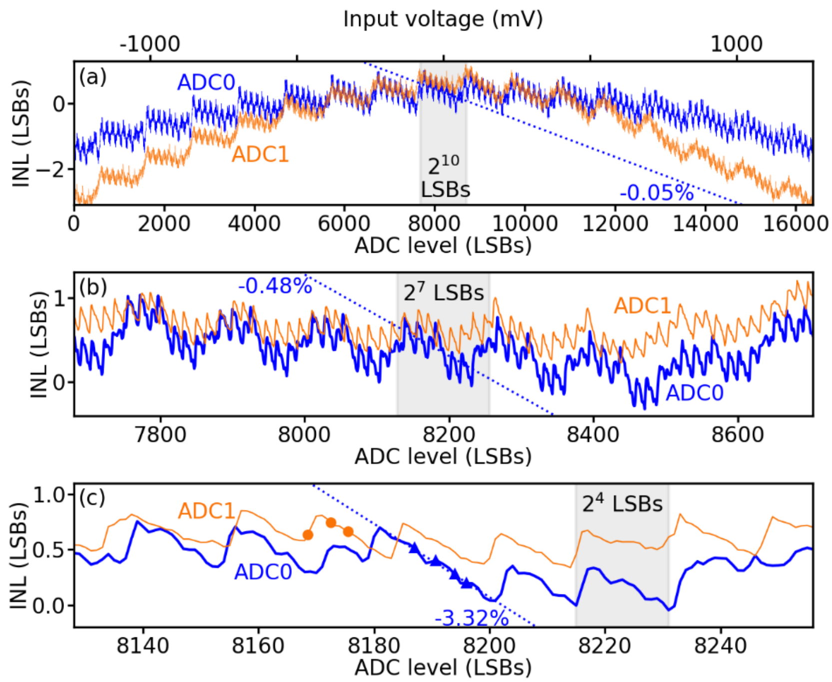

Fig. 3. Integrated nonlinearity (INL) plot for two ADCs shows a sawtooth pattern of digitization error as a function of input voltage. 0 LSB corresponds to −1.285 V and 16384 LSB to +1.285 V. (a) Over the full voltage range, the dominant sawtooth pattern has a period of 10 bits (gray-shaded region) and an overall slope (dotted line), or gain error, of −0.05% around 8192 LSB or nominally 0 V. (b) Inset of (a) over the 10-bit region reveals a second sawtooth pattern at 7 bits and a larger slope of −0.48%. (c) Inset of (b) over 7-bit region shows sawtooth at 4 bits and −3% slope. The exact zero-voltage level can change in the ADC and observed values are shown as triangles (ADC0) and circles (ADC1).

3. Demonstration and theory of digitizer-induced bias

The impact of this digitizer nonlinearity on DCS can be seen by measuring absorption features in a CH_4 cell on two separate digitizers (Fig. 4(a)). Here a resistive splitter is used to route a detected DCS heterodyne signal from the photodetector onto the two ADC channels whose INL is characterized in Fig. 3. The DCS consists of two optical frequency combs with repetition rates around 200 MHz and a 416 Hz difference in repetition rates. The CH_4 cell is 5.5 cm long and filled to 100 hPa with pure CH_4. In this example, the 120 µW of chirped DCS light on the detector only fills 2% or 320 LSBs of the ADC range after being split between the two digitizers (Fig. 4(b)). (While small, such signal levels can be encountered in open path spectroscopy where link loss can fluctuate by many dB, so most of the digitizer range is reserved to accommodate the extremums.) A field-programmable gate array (FPGA) phase-corrects and coadds 40,000 of these digitized interferograms for 96 seconds [23] to smooth out the ADC quantization levels using the >1 LSB random noise at the digitizer input. To extract CH_4 concentration, we fit each 96-second spectrum [25] using HITRAN2020 [26] across the 1650 nm CH_4 absorption band. Figure 4(d) shows that the concentrations retrieved from the two ADC channels (ADC 0 and ADC 1) are systematically offset by 3%, despite sharing the same optical path and photodetector.

To understand the mechanism for this ADC-dependent concentration bias, we must consider the time-domain interferogram signal that the ADC digitizes. The interferogram has two components: the high-amplitude centerburst, followed by the weaker ringing of the excited molecules known

Optics EXPRESS

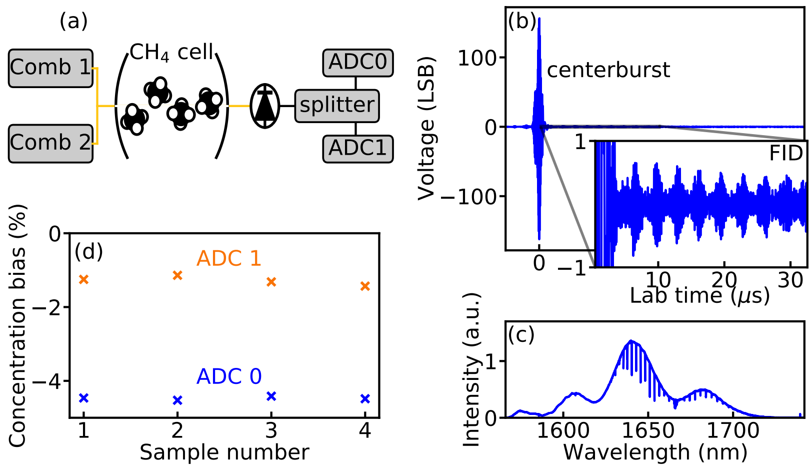

Fig. 4. (a) Experimental setup to compare concentration measurements with multiple digitizers (ADCs). A DCS setup is used to measure a methane gas cell. The resulting interferogram is split with a resistive splitter and digitized on two separate ADCs. Yellow lines: fiber optics; black lines: RF cabling. (b) Chirped interferogram measured on ADC, where the centerburst amplitude is 300× the free induction decay (FID) amplitude. (c) Corresponding spectrum to fit. (d) Sequential DCS measurements on each ADC produce a persistently different CH_4 concentration measurement.

as free-induction decay (FID) which may only be a few LSBs in amplitude (Fig. 4(b)). To first order, the measured gas concentration is proportional to the relative size of the centerburst and FID. While the INL of our ADCs seldom exceeds 1 bit-level over the full voltage range, over small voltage ranges INL can have slope errors around −3% (Fig. 3(c)), which would compress the FID amplitude but not the larger centerburst. This −3% slope error is roughly consistent with the bias shown in Fig. 4(d). ADC0 shows larger bias since the ADC level associated with a zero-volt input sits near the middle of a particularly large sawtooth period (Fig. 3(c)). Both ADCs have negative bias because the INL slope is typically negative. For most of this paper we will focus on ADC0 since it shows a more severe bias.

In summary, bias arises when the FID of a high-contrast interferogram is contained within a smaller-voltage, greater-error sawtooth period than the centerburst. This mechanism for digitizer-induced bias is thus different than for cavity-ringdown absorption measurements [27], as a low-order polynomial correction to the INL will not reduce the concentration bias. Instead, we will add RF electronics to mitigate the bias.

4. Mitigating digitizer nonlinearity

To develop mitigation approaches for this bias, we perform a series of gas cell measurements while applying noise or dither to “wash out” the ADC INL structure through averaging. We also match the measurement conditions in accompanying simulations to isolate the digitizer contribution to bias.

The simulation starts with a zero-noise interferogram: we approximate the laser spectral shape measured in Fig. 4(c) as a sum of three Gaussians, multiply that by the negative exponential of the HITRAN methane absorbance model, add a spectral phase corresponding to ∼1 m of differential fiber chirp, and inverse Fourier transform the result. We scale this interferogram to a peak-to-peak level of 320 LSBs, add Gaussian noise with a standard deviation of 1.1 LSBs to match the observed interferogram, and add any additional dither signal for nonlinearity mitigation. We then apply the transfer function, H_{ADC}, to digitize this interferogram. Just as with the lab

Optics EXPRESS

measurement, ~40,000 interferograms are coadded, each with a different noise and dither signal realization.

In previous DCS work [17,18], a simple 1 MHz sinewave dither was added to the signal prior to digitization to remove bias. We compare experimental results to the simulation as a function of dither amplitude in Fig. 5. The simulations match the cell data with an R^2 of 0.85, indicating that the simulations capture the relevant bias processes. Because the zero voltage level drifts, the simulations are performed for a range of zero-voltage levels in addition to the zero-voltage level associated with the data. All converge to a similar behavior at larger modulations.

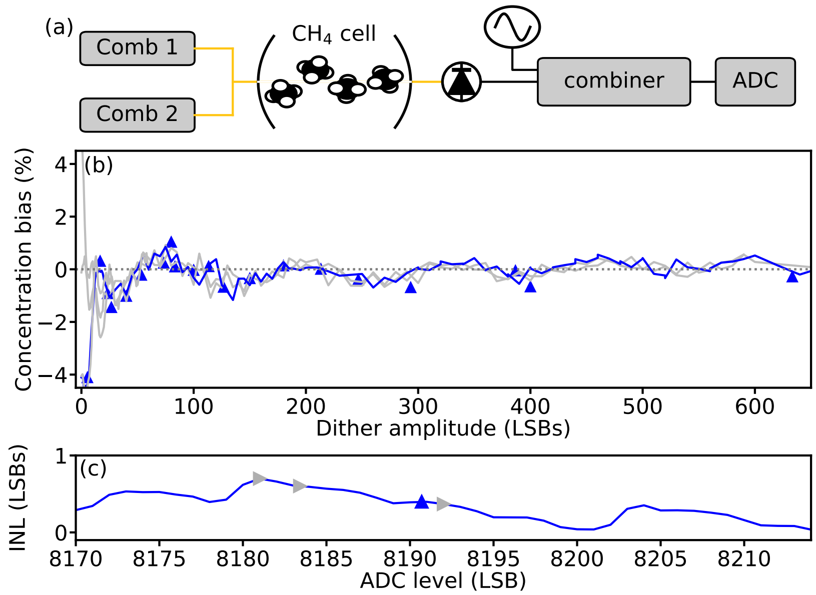

Fig. 5. (a) Experimental setup to suppress the digitizer bias by adding a 1 MHz sinewave dither to the photodetected signal. (b) CH_4 retrievals converge toward the expected concentration for experimental data (blue triangles) and simulated spectra at observed zero-voltage level (blue line) and other zero-voltage levels (grey lines). (c) The INL curve from Fig. 3 with markers indicating the zero-voltage levels used for the simulations in (b).

Though the sinewave dither reduces the ADC-induced bias, the concentration bias also continues to oscillate at 0.5% bias out to large dither amplitudes, suggesting that sinewave dither is not an optimal solution. The period and amplitude of this oscillation matches the 128 LSB sawtooth structure shown in Fig. 3(b). Another potential drawback of this approach is that the INL will also act on the dithering sinewave and will generate harmonics that might distort the spectrum. Choosing a sinewave at the sampling frequency would mitigate this harmonics problem.

4.1. Bias removal through optical chirping and RF amplifying the interferogram

Recall in Fig. 3(b) that signal amplitudes below 128 LSBs (20 mV) may experience a −0.5% bias on our ADC. Therefore, to achieve sub-0.5% concentration bias, we expect that our interferogram tail (FID and additive white noise) should exceed this amplitude.

For a typical DCS this requires considerable amplification. Assume the white noise on the interferogram comes from an amplified photodetector with detector noise of 13 pW/$\sqrt{\text{Hz}}$ (~10× the thermal noise limit) and a 50 Ω-impedance gain of 5 kV/W; after low-pass filtering the interferogram and noise at a bandwidth of half the sampling frequency (here $f_s/2 = 100$ MHz), that noise has a standard deviation of only 650 μV or 4 LSBs, thus additional RF gain is required. However, with added RF gain, care must be taken to avoid saturating the large interferogram centerburst. Here we reduce the centerburst amplitude ~10× by increasing the relative chirp between the two combs, introducing 3 m of 18 ps/(nm km) supplemental fiber in one of the interferometric arms.

Just as for sinewave dither, we test this approach on both cell measurements and simulations. We report the net gain of a varying chain of RF amplifiers and attenuators, and also record the standard deviation of the raw ADC measurement away from the centerburst. As can be seen in Fig. 6, the agreement between model and measurements for both ADCs is quite good ($R^2 = 0.83$), though for the experimental data the actual concentration of CH_4 in the cell is not known to 0.1% so we take the highest-gain data point from ADC1 to be the actual CH_4 concentration. Unlike the sinewave dither, which oscillates up to 0.5% bias (Fig. 5), this amplification approach asymptotes to 0.1% bias at high RF gain.

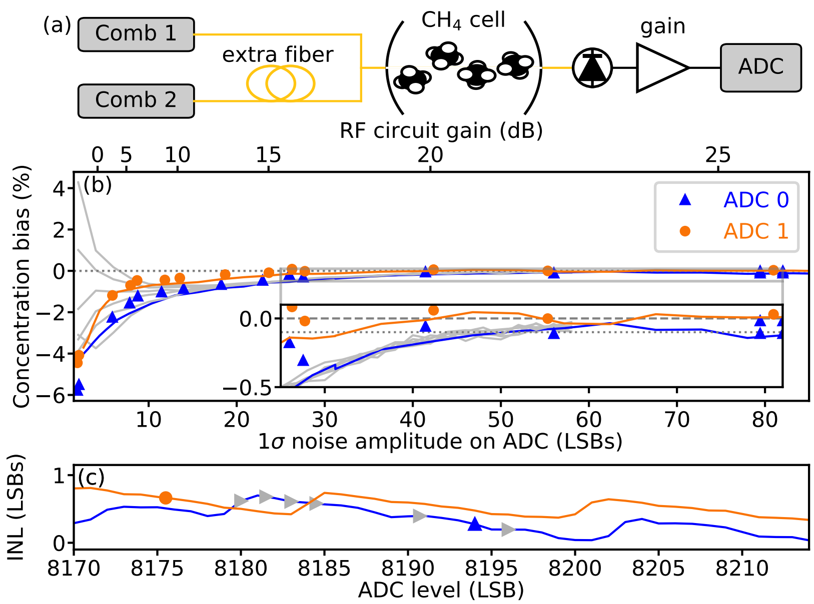

Fig. 6. (a) Experimental setup to suppress the digitizer bias by including differential chirp to reduce the photodetected signal amplitude, followed by RF amplifying both the signal and noise. Approximately 0.06 ps/nm of fiber dispersion was added to one comb in both experiment and simulation. The corresponding chirp spreads out the interferogram in time and avoids overfilling the ADC. (b) Concentration bias as a function of the amplified noise levels (bottom axis) or RF gain (top axis) for two different ADCs (triangle and circles) and simulation (lines). The bias drops below 0.1% (inset, dotted line) only when the measurement noise is amplified above 45 LSBs standard deviation. (c) The measured INL for the two ADCs (solid lines) and the zero-voltage levels (colored symbols) recorded for the cell data in (b). Simulations at different zero-voltage levels (grey triangles) yielded the additional (grey) curves in (b).

While this approach achieves consistently low bias at high amplification, it has its drawbacks. To achieve sub-0.1% concentration biases, the interferogram must be chirped so that noise can be amplified above 45 LSBs standard deviation (roughly the amplitude where a ± 2σ peak-to-peak noise overfills the 128 LSB sawtooth period). As this solution of increasing the gain is multiplicative, $\log_2(45) = 5.5$ ADC bits are lost to amplify random noise such that it can sufficiently dither the INL structure. This means that 8.5 bits out of 14 are effectively left to

Research Article | Vol. 31, No. 18 / 28 Aug 2023 / Optics Express 29081
Optics EXPRESS

digitize the signal, a figure significantly smaller than the 14-bit range or even the quoted 11.3 bits ENOB of this digitizer. For most DCS systems, this will require applying differential chirp or reducing the bandwidth to reduce the interferogram contrast and avoid overfilling the ADC. While some DCS applications could work within this remaining range, applications sampling turbulent environments such as long open-air paths [17,24] or combustion measurements [12,14,28] need to reserve much of the ADC range to handle signal fluctuations and would not be compatible with this approach.

Strongly chirping the interferogram also comes with drawbacks: laser intensity noise is mapped to spectral fluctuations, and chirp can be difficult to implement in DCS systems operating at wavelengths where dispersive optical fibers are lossy or nonexistent, such as mid-infrared and UV.

4.2. Bias removal through added band-limited noise

To relax this dynamic range constraint, one can instead add out-of-band noise as an effective dither. Provided that it is narrow band around the sampling (f_s) or the Nyquist ($f_s/2$) frequency, this addition does not impact the DCS signal as all harmonics of the dither signal fall around 0 Hz or f_s / 2 Hz respectively [29,30]. We experimentally implemented band-limited noise with three analog amplifiers into a 5%-width bandpass filter, although it could also be implemented with a digital-to-analog converter. We both measure and simulate adding band-limited noise from 95-100 MHz and find (Fig. 7) that the concentration bias converges smoothly below 0.1% here as well. This 0.1% bias occurs when the noise standard deviation exceeds 45 LSBs on the ADC, corresponding to a power of −36 dBm out of the 5 MHz bandpass filter.

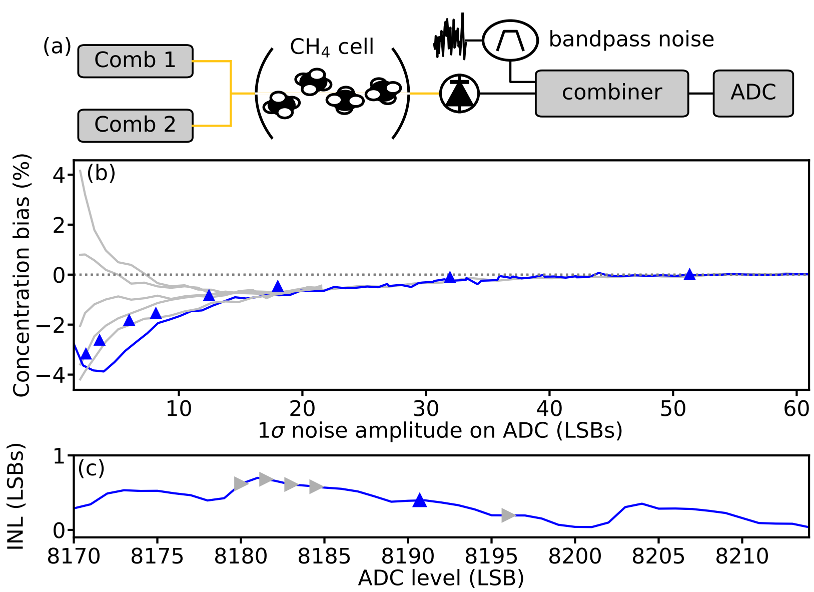

Fig. 7. (a) Experimental setup to suppress the digitizer bias by adding bandwidth-limited noise to the photodetected signal. (b) Concentration bias as a function of band-limited noise amplitude for measurements (blue triangles) and simulations (blue and gray traces). (c) The corresponding INL (blue trace) and zero-voltage input levels (triangles) input into the simulation to generate the bias curves shown in (b). Upward-pointing blue triangle indicates zero-voltage recorded during cell measurements.

In fact, the band-noise simulations in Fig. 7 are nearly identical to the amplifier simulation traces in Fig. 6, even though the unamplified FID signal is weaker. This equivalence indicates

Optics EXPRESS

that the time-domain noise standard deviation is the critical parameter to reduce concentration bias, regardless of how the noise is generated.

The advantage band limited noise has over the amplification approach is that it is additive instead of multiplicative with respect to the actual IGM signal, and thus uses up a negligible fraction of the ADC bit range. At 45 LSBs of additive noise, the ADC still has 13.9 bits left for the signal and the concentration bias drops below 0.1% even with an interferogram amplitude as low as 250 LSB_{pp} and a sub-LSB FID amplitude. These 13.9 bits exceed the 11.3 ENOB of this device, showing that the band-limited approach functionally recovers extra ADC range.

4.3. Other dither approaches

It is worth noting that there are a number of other modulation approaches one could apply. We have shown a few promising ones here and we also demonstrate a reliable model that could be used to evaluate other modulations.

For instance, bias could be mitigated by applying extremely narrowband noise centered around the sampling frequency such that the dithering signal changes slowly over an interferogram. This would effectively add a dither signal that passes through any AC-coupling filter but uses only a negligible band around DC after sampling. Functionally this would modulate the DC value of each interferogram to remove the INL structure. Other options include applying a slowly-varying DC offset after the AC coupling, or modulating a sinewave with a triangle wave at 100% modulation amplitude.

5. Summary and outlook

The moderately high speed and high bit-depth requirements for dual-comb spectroscopy pushes much of the field toward pipeline ADCs which can have strong gain errors over small voltage ranges, resulting in large biases of retrieved species concentrations. Here we show two possible strategies to mitigate these biases and support DCS concentration measurements at the 0.1% level. Of the two, the additive band-limited noise approach is the most general and will work at optical frequencies that cannot easily be chirped, or in the presence of strong power fluctuations. In both mitigation approaches, the optimal dither conditions can be determined either by measuring the INL and setting the peak-to-peak noise amplitude above the sawtooth period, or by experimentally increasing the noise level on the ADC until extracted concentration values become constant.

Forgoing the mitigation steps shown here and applying a bias correction directly to the measured concentration is hypothetically possible, but the correction will change with the drifting zero-voltage level and potentially with changes in signal level. It may be difficult to do this in a way that is robust and universal.

We implicitly consider mode-locked laser based dual-comb where high contrast interferograms (like Fig. 4(b)) are standard, but EO comb and micro-comb platforms with sufficiently broad bandwidth can also be affected by ADC nonlinearities. Dual-comb spectroscopy performed with quantum cascade laser combs may find it easier to suppress INL effects, since the interferogram generated by these systems is spread out in time and need only be sufficiently amplified. Alternatively, dual-comb systems that down-convert the spectrum to a sufficiently low bandwidth [31,32] could rely on more linear Sigma-Delta ADCs, although they are limited to sampling rates below ~1 MS/s [15], which is insufficient for most DCS systems.

The dither-and-coadd approach shown here is analogous to the principle behind the high linearity of Sigma-Delta ADCs. The reason Sigma-Delta ADCs are slow is that during each sample the ADC mixes the input signal with a sequence of random voltages at the LSB level. Over enough cycles of the digital mixing voltage, the effect on the input voltage averages to zero. Whereas the Sigma-Delta ADC effectively dithers and averages each point on the signal before moving chronologically to the next point, we measure the entire interferogram before repeating the same measurement with a different dither realization.

While this work was performed with a specific ADC, we expect it will be broadly applicable. First, the ADC examined here has been used in a number of dual-comb measurements that we know of, for example Refs. [17,22–24,28]. Furthermore, this nested sawtooth structure does seem to be common among pipeline ADCs [19], although the exact sawtooth periods may vary.

Lastly, we have looked at the impact of ADC INL on other absorption parameters besides concentration, but in these cases the impact is muted. In the simple model ADC nonlinearity primarily changes the depth of each absorption feature, so concentration and line intensities are affected, but the same fractional intensity change is imposed across the entire spectrum. Therefore, other parameters such as temperature and pressure are substantially less sensitive to ADC nonlinearity.

Funding. Air Force Office of Scientific Research (MIPR12953278); National Aeronautics and Space Administration; National Institute of Standards and Technology.

Acknowledgments. The authors thank Adam Fleischer and Dohyeon Kwon for instructive comments.

Disclosures. The authors declare no conflicts of interest. Official contribution of the National Institute of Standards and Technology; not subject to copyright in the United States.

Data availability. Data underlying the results presented in this paper are available in Dataset 1, Ref. [33].

References

1. I. Coddington, N. Newbury, and W. Swann, "Dual-comb spectroscopy," Optica **3**(4), 414–426 (2016).
2. I. Coddington, W. C. Swann, and N. R. Newbury, "Time-domain spectroscopy of molecular free-induction decay in the infrared," Opt. Lett. **35**(9), 1395–1397 (2010).
3. D. B. Chase, "Nonlinear detector response in FT-IR," Appl. Spectrosc. **38**, 73 (1975).
4. P. Hoffmann and E. Knözinger, "Dynamic Range Problems in Fourier Transform IR and Far-IR Spectroscopy," Appl. Spectrosc. **41**(8), 1303–1306 (1987).
5. P. R. Griffiths and J. A. de Haseth, "Sampling the interferogram," in *Fourier Transform Infrared Spectroscopy*, 2nd ed. (Wiley, 2007), pp. 64–74.
6. P. Guay, A. Tourigny-Plante, V. Michaud-Belleau, V. Michaud-Belleau, N. B. Hébert, N. B. Hébert, A. Gouin, and J. Genest, "Understanding photodetection nonlinearity in dual-comb interferometry," OSA Continuum **4**(9), 2460–2467 (2021).
7. A. Crotwell and M. Steinbacher, and World Meteorological Organization, *19th WMO/IAEA Meeting on Carbon Dioxide, Other Greenhouse Gases and Related Measurement Techniques* (2018), p. 2.
8. X. Zhao, G. Hu, B. Zhao, C. Li, Y. Pan, Y. Liu, T. Yasui, and Z. Zheng, "Picometer-resolution dual-comb spectroscopy with a free-running fiber laser," Opt. Express **24**(19), 21833–21845 (2016).
9. B. Lomsadze and S. T. Cundiff, "Frequency combs enable rapid and high-resolution multidimensional coherent spectroscopy," Science **357**(6358), 1389–1391 (2017).
10. A. Asahara and K. Minoshima, "Development of ultrafast time-resolved dual-comb spectroscopy," APL Photonics **2**(4), 041301 (2017).
11. R. Liao, Y. Song, W. Liu, H. Shi, L. Chai, and M. Hu, "Dual-comb spectroscopy with a single free-running thulium-doped fiber laser," Opt. Express **26**(8), 11046–11054 (2018).
12. M. A. Abbas, L. van Dijk, K. E. Jahromi, M. Nematollahi, F. J. M. Harren, and A. Khodabakhsh, "Broadband Time-Resolved Absorption and Dispersion Spectroscopy of Methane and Ethane in a Plasma Using a Mid-Infrared Dual-Comb Spectrometer," Sensors **20**(23), 6831 (2020).
13. K. Hashimoto, V. R. Badarla, T. Imamura, and T. Ideguchi, "Broadband complementary vibrational spectroscopy with cascaded intra-pulse difference frequency generation," Opt. Lett. **46**(21), 5517–5520 (2021).
14. R. T. Rhoades, R. R. D. Weeks, S. E. Erickson, C. Lecaplain, S. S. Harilal, M. C. Phillips, and R. J. Jones, "Dual-comb absorption spectroscopy of molecular CeO in a laser-produced plasma," Opt. Lett. **47**(10), 2502–2505 (2022).
15. W. Kester, "Which ADC Architecture Is Right for Your Application?" https://www.analog.com/en/analog-dialogue/articles/the-right-adc-architecture.html.
16. S. Arar, "Understanding ADC Integral Nonlinearity (INL) Error," https://www.allaboutcircuits.com/technical-articles/understanding-analog-to-digital-converter-integral-nonlinearity-inl-error/.
17. E. M. Waxman, K. C. Cossel, G.-W. Truong, F. R. Giorgetta, W. C. Swann, S. Coburn, R. J. Wright, G. B. Rieker, I. Coddington, and N. R. Newbury, "Intercomparison of open-path trace gas measurements with two dual-frequency-comb spectrometers," Atmos. Meas. Tech. **10**(9), 3295–3311 (2017).
18. N. A. Malarich, B. R. Washburn, K. C. Cossel, G. J. Mead, F. R. Giorgetta, D. I. Herman, N. R. Newbury, and I. Coddington, "Validation of open-path dual-comb spectroscopy against an O_2 background," Opt. Express **31**(3), 5042–5055 (2023).
19. S. Medawar, P. Händel, N. Björsell, and M. Jansson, "ADC characterization by dynamic integral nonlinearity," in *13th Workshop on ADC Modeling and Testing* (2008), pp. 1–6.

Optics EXPRESS

20. "IEEE Standard for Terminology and Test Methods for Analog-to-Digital Converters," IEEE Std 1241-2010 Revis. IEEE Std 1241-2000 1–139 (2011).
21. Certain equipment or instruments are identified in this paper in order to specify the experimental procedure adequately. Such identification is not intended to imply recommendation or endorsement of any product by NIST, nor is it intended to imply that the equipment identified are necessarily the best available for the purpose.
22. J. Roy, J.-D. Deschênes, S. Potvin, and J. Genest, "Continuous real-time correction and averaging for frequency comb interferometry," Opt. Express **20**(20), 21932–21939 (2012).
23. G. Ycas, F. R. Giorgetta, E. Baumann, I. Coddington, D. Herman, S. A. Diddams, and N. R. Newbury, "High-coherence mid-infrared dual-comb spectroscopy spanning 2.6 to 5.2 µm," Nat. Photonics **12**(4), 202–208 (2018).
24. S. Coburn, C. B. Alden, R. Wright, K. Cossel, E. Baumann, G.-W. Truong, F. Giorgetta, C. Sweeney, N. R. Newbury, K. Prasad, I. Coddington, and G. B. Rieker, "Regional trace-gas source attribution using a field-deployed dual frequency comb spectrometer," Optica **5**(4), 320–327 (2018).
25. R. K. Cole, A. S. Makowiecki, N. Hoghooghi, and G. B. Rieker, "Baseline-free quantitative absorption spectroscopy based on cepstral analysis," Opt. Express **27**(26), 37920–37939 (2019).
26. I. E. Gordon, L. S. Rothman, and R. J. Hargreaves, *et al.*, "The HITRAN2020 molecular spectroscopic database," J. Quant. Spectrosc. Radiat. Transfer **277**, 107949 (2022).
27. A. J. Fleisher, E. M. Adkins, Z. D. Reed, H. Yi, D. A. Long, H. M. Fleurbaey, and J. T. Hodges, "Twenty-Five-Fold Reduction in Measurement Uncertainty for a Molecular Line Intensity," Phys. Rev. Lett. **123**(4), 043001 (2019).
28. D. Yun, R. K. Cole, N. A. Malarich, S. C. Coburn, N. Hoghooghi, J. Liu, J. J. France, M. A. Hagenmaier, K. M. Rice, J. M. Donbar, G. B. Rieker, and G. B. Rieker, "Spatially resolved mass flux measurements with dual-comb spectroscopy," Optica **9**(9), 1050–1059 (2022).
29. L. Melkonian, *Improving A/D Converter Performance Using Dither* (National Semiconductor, 1992).
30. B. Brannon, *Overcoming Converter Nonlinearities with Dither* (Analog Devices, 1995).
31. P. Martín-Mateos, F. U. Khan, and O. E. Bonilla-Manrique, "Direct hyperspectral dual-comb imaging," Optica **7**(3), 199–202 (2020).
32. T. Voumard, T. Wildi, V. Brasch, R. G. Álvarez, G. V. Ogando, and T. Herr, "AI-enabled real-time dual-comb molecular fingerprint imaging," Opt. Lett. **45**(24), 6583–6586 (2020).
33. N. Malarich, "Dataset 1," figshare (2023). https://doi.org/10.6084/m9.figshare.23841900.